Astron. Astrophys. 324, 203–210 (1997)

ASTRONOMY AND ASTROPHYSICS

Four dense molecular cores in the Taurus Molecular Cloud (TMC)

Ammonia and cyanodiacetylene observations

C. Codella[1], **R. Welser**[1], **C. Henkel**[1], **P.J. Benson**[2], **and P.C. Myers**[3]

[1] Max-Planck-Institut für Radioastronomie, Auf dem Hügel 69, D-53121 Bonn, Germany
[2] Whitin Observatory Wellesley, Wellesley, Massachusetts 02181, USA
[3] Harvard-Smithsonian Center for Astrophysics, 60 Garden Street, Cambridge, MA 02138, USA

Received 12 July 1996 / Accepted 7 January 1997

Abstract. Trying to obtain a more complete picture of star forming regions in the Taurus molecular cloud, four dense molecular cores (L1521D, L1521F, L1524, L1507A) are identified and mapped through the ammonia (J,K) = (1,1) and (2,2) rotational inversion lines. These cores have sizes from 0.06 to 0.09 pc, hydrogen densities from 0.6 10^4 to 19.9 10^4 cm^{-3} and kinetic temperatures between 7.9 and 9.9 K. The masses range from 0.2 and 1.0 $M_\odot$, placing the cores with the lowest M values at the lower edge of the mass distribution for ammonia cores in the TMC. Turbulent, thermal and gravitational energies have been estimated. A comparison between these energy terms and considerations related to thermal and turbulent line broadening indicate that these cores are close to gravitational equilibrium. Moreover, we report detections of the J=9–8 transition of HC_5N towards the ammonia peak positions of these four molecular cores. The HC_5N column densities are between 1.6 10^{12} and 9.2 10^{12} cm^{-2}, in agreement with values derived for other molecular cores located in the TMC.

Key words: ISM: clouds – ISM: molecules – radio lines: ISM – ISM: individual objects: TMC

1. Introduction

The Taurus molecular cloud (TMC) is one of the best targets to study low-mass star formation, since it is located at a distance of only 140 pc. The region is associated with T Tauri stars, identified by infrared and optical observations (e.g. Strom et al. 1989; Kenyon et al. 1990; Weintraub 1990), low-luminosity objects extracted from the IRAS Point Source Catalogue (PSC, IRAS 1985), molecular outflows (e.g. Fukui 1989; Fukui et al. 1993) and water maser sources (Wouterloot et al. 1993), indicating ongoing star formation. The TMC contains several dark molecular clouds of size $\simeq$ 1 pc and densities of 10^3 cm^{-3} (e.g. Walmsley et al. 1980; Wouterloot & Habing 1985; Ungerechts & Thaddeus 1987; Mizuno et al. 1995). These in turn contain dense molecular cores, high density ($\geq 10^4$ cm^{-3}) substructures which have been classified by Myers et al. (1983) and Myers & Benson (1983). For the sky distribution of the molecular cores in the TMC, see Kenyon et al. (1990). Subsequent multimolecular observations (e.g. Benson & Myers 1984; Fuller 1989; Fuller & Myers 1993) have confirmed that dense cores are smaller than 0.1 pc with masses ranging from 0.5 to 10 solar masses and kinetic temperatures of the order of 10 K. Beichman et al. (1984; 1986) have shown that about 50% of the molecular cores are associated with IRAS sources, indicating that these objects may contain, in their interiors, young stellar objects (YSOs). Therefore, it is now clear that there exists a close association between low-mass YSOs and molecular clumps. Since the TMC is not strongly affected by the nearby Cas-Tau OB association (Blaauw 1991), it is clear that it provides unique opportunities to study spontaneous low-mass star formation and, in particular, to investigate the nature of the earliest stages of low-mass star formation, strictly connected with dense molecular clumps.

Following the definition given by Myers & Benson (1983; i.e. sources with $T_A^* \geq 0.4$ K at the Haystack and Green Bank antennas), 16 dense molecular cores have so far been identified in the TMC (Myers & Benson 1983; Benson & Myers 1989). In order to obtain a more complete sample of TMC cores, to gain information about the nature of the molecular gas before or at the onset of YSO formation and to clarify the evolutionary stages connected with the collapse process, we report observations of the NH_3 (J, K) = (1,1) and (2,2) inversion lines and the cyanodiacetylene (HC_5N) J=9–8 rotational line towards 4 newly discovered dense cores.

2. Selection criteria

The molecular cores chosen for this project have been selected from an extensive search for ammonia emission towards 26 high

Send offprint requests to: C. Henkel

Table 1. Regions investigated through NH_3 observations

α (1950)	δ (1950)	T_A^* (mK)	Antenna [a]	Dense core
04 17 56	+26 55 23	449	GB	L 1521 D
04 18 55	+29 21 00	< 95	HA	
04 19 55	+19 19 49	< 102	GB	
04 20 30	+26 32 47	< 101	GB	
04 21 48	+27 10 58	< 95	GB	
04 23 36	+24 32 40	< 150	HA	
04 25 00	+18 35 12	< 103	GB	
04 25 35	+26 45 00	977	GB	L 1521 F
04 26 20	+24 28 06	603	GB	L 1524
04 26 25	+26 52 47	< 102	GB	
04 27 58	+24 21 06	< 113	HA	
04 28 02	+24 05 20	< 108	HA	
04 28 40	+27 02 13	< 85	GB	
04 29 38	+24 42 13	< 80	HA	
04 29 40	+24 06 00	< 151	HA	
04 29 57	+24 10 53	< 179	HA	
04 31 08	+24 02 10	216	GB	
04 32 37	+24 01 42	788	HA	L 1535
04 37 28	+29 50 00	< 74	HA	
04 37 39	+29 48 37	270	GB	
04 39 29	+29 38 07	472	GB	L 1507 A
04 40 20	+29 34 37	276	GB	
04 42 18	+16 31 58	< 85	GB	
04 42 22	+17 01 42	< 86	GB	
04 42 38	+16 51 35	< 85	GB	
04 57 16	+26 10 23	236	GB	

[a] Observed with the 43-m Green Bank antenna (GB) or with the 37-m Haystack antenna (HA) in 1983. The FWHP beam sizes are $\simeq$ 84 arcsec, while the beam efficiencies are $\simeq$ 0.25.

visual extinction regions in the TMC identified from the Palomar Observatory Sky Survey (POSS) maps and from Myers et al. (1979). The observed positions are located within $04^h\ 15^m \leq \alpha \leq 05^h\ 00^m$ and $+16^\circ \leq \delta \leq +30^\circ$: 9 regions in the long filament which includes TMC-2 (Kutner's Cloud), 7 regions in the parallel filament to the north, containing B217 (see Fig. 1 of Walmsley et al. 1980), and 10 isolated optically obscured regions where no extended clouds were seen on the POSS plates. For the survey, the Haystack (USA) 37-m and the Green Bank (USA) NRAO 43-m antennas have been used with FWHP (full width half power) beam sizes of $84''$ and beam efficiencies of about 0.25 during several runs in 1983.

Table 1 summarizes the regions where NH_3 line emission was searched for. For the non-detections the r.m.s. T_A^* value is reported. Ammonia emission has been detected towards 9 sources. Out of these 9, 5 can be classified as dense molecular cores: L1521D, L1521F, L1524, L1535 and L1507A. L1521D, L1521F and L1524 have been already studied through $H^{13}CO^+$ and $C^{18}O$ observations by Mizuno et al. (1994) and Onishi et al. (1996). Since L1535 has already been investigated by Ungerechts et al. (1982), through ammonia observations, we have focused our attention on the other four cores, which have been mapped in NH_3, using the 100-m MPIfR radio-telescope at Effelsberg (Germany).

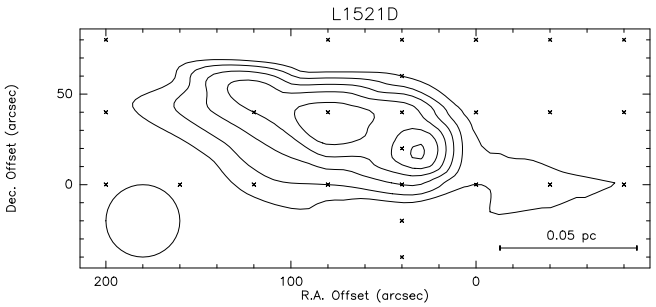

Fig. 1. Contour NH_3 (1,1) T_{MB} map of L1521D. The (0,0) position corresponds to: $\alpha = 04^h\ 17^m\ 56^s$; $\delta = +26^\circ\ 55'\ 23''$. The contour levels are from 1.4 K to 2.4 K by steps of 0.2 K ($\simeq$ 1 r.m.s. noise). The empty circle shows the Effelsberg beam (HPBW), the small crosses mark measured positions.

3. Observations

The observations were made during several runs in 1985, 1986 and 1996 with the MPIfR antenna employing a maser receiver during the 1985-1986 and a HEMT receiver during the 1996 periods. At the rest frequency of the $(J, K) = (1,1)$ and (2,2) lines of NH_3 (23694.496 MHz and 23722.631 MHz, respectively) and of the J=9–8 line of HC_5N (23963.888 MHz) the FWHP beam size is $40''$. The zenith system temperature was around 60 K in good weather conditions on an atmosphere corrected antenna temperature (T_A^*) scale. The observations were made using position switching, with an integration time of typically 3 minutes on source. Spectral information was obtained with a 1024–channel three–level autocorrelation spectrometer. We observed the NH_3 (1,1) and (2,2) lines simultaneously by splitting the autocorrelator into two spectrometers of 512 channels with bandwidths of 6.25 MHz and channel spacings of 0.154 km s^{-1}. The velocity resolution was 0.185 km s^{-1}, i.e. a factor 1.2 larger than the channel spacing. We observed the HC_5N line with the autocorrelator split into two parts, each with a bandwidth of 3.12 MHz and a velocity resolution of 0.092 km s^{-1}. The spectra from the two split parts were then co-added in order to reduce the noise. The intensity scale of the spectra was calibrated on the continuum sources NGC7027, 3C123 and 3C286, according to the flux densities given by Baars et al. (1977). The pointing accuracy was better than $10''$, corresponding to a point source flux density error of $< 15\%$. The calibration accounted for the dependence of the gain on the elevation. Total flux density uncertainties are of the order of 20%.

4. Results

Ammonia maps have been obtained of the four dense cores L1521D, L1521F, L1524 and L1507A in the $(J, K) = (1,1)$ line (Figs. 1 to 4). In order to obtain the observed source size, we have determined the half maximum contours of the ammonia main beam brightness temperature (T_{MB}; K) and have calculated the apparent geometric mean diameter (FWHP) $D = \sqrt{ab}$, where a and b are the major and minor-axis, respectively. The ammo-

Table 2. Observed NH_3 (1,1) line parameters. The (1950) coordinates of the peak positions of the four cores are: ($\alpha = 04^h\ 17^m\ 59^s$; $\delta = +26^\circ\ 55'\ 43''$) and ($\alpha = 04^h\ 18^m\ 02^s$; $\delta = +26^\circ\ 56'\ 03''$) for L1521D, ($\alpha = 04^h\ 25^m\ 36^s$; $\delta = +26^\circ\ 45'\ 00''$) for L1521F, ($\alpha = 04^h\ 26^m\ 21^s$; $\delta = +24^\circ\ 28'\ 26''$) for L1524 and ($\alpha = 04^h\ 39^m\ 29^s$; $\delta = +29^\circ\ 38'\ 17''$) for L1507A

Name	$\Delta\alpha$ ($''$)	$\Delta\delta$ ($''$)	T_{MB} (K)	v_{LSR} (km s^{-1})	FWHM (km s^{-1})	τ_{tot}	Δv_{INT} (km s^{-1})
L1521D	+40,	+20	2.3 (0.1)	6.94 (0.15)	0.8 (0.2)	4.5 (1.1)	0.33 (0.02)
	+80,	+40	2.3 (0.1)	6.97 (0.15)	0.6 (0.2)	4.6 (1.3)	0.30 (0.02)
L1521F	+20,	0	6.1 (0.3)	6.62 (0.15)	0.7 (0.2)	12.0 (0.8)	0.25 (0.01)
L1524	+20,	+20	4.7 (0.2)	6.40 (0.15)	0.8 (0.2)	14.0 (0.9)	0.26 (0.01)
L1507A	0,	+10	3.4 (0.2)	6.16 (0.15)	0.7 (0.2)	5.8 (0.9)	0.27 (0.01)

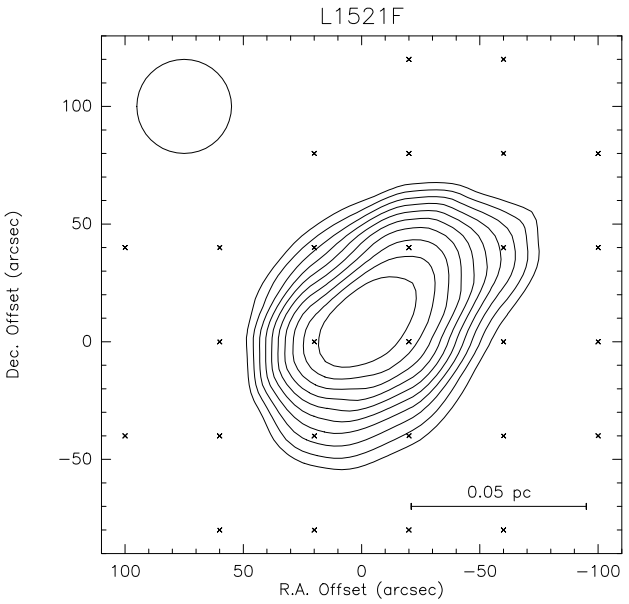

Fig. 2. Contour NH_3 (1,1) T_{MB} map of L1521F. The (0,0) position corresponds to: $\alpha = 04^h\ 25^m\ 35^s$; $\delta = +26^\circ\ 45'\ 00''$. The contour levels are from 2.6 K to 6.4 K by steps of 0.4 K ($\simeq$ 2 r.m.s. noise). The empty circle shows the Effelsberg beam (HPBW).

nia core sizes are 0.09 pc (L1521D), 0.07 pc (L1521F), 0.08 pc (L1524) and 0.06 pc (L1507A). Deconvolution by the 0.027 pc beam does not significantly alter these values. For those spectra where the main and satellite hyperfine components have been observed with a sufficient signal-to-noise ratio (> 3) we have obtained the total optical depth (τ_{tot}) and the intrinsic linewidth (FWHM) of the hyperfine components (Δv_{INT}; km s^{-1}) using a program which fits these parameters to the observed spectra, assuming gaussian profiles in an individual component and relative opacities being consistent with the Local Thermodynamic Equilibrium (LTE) approximation. For the positions where the satellite components have intensities below the noise level, but the main component of the NH_3 (1,1) line has been detected, we have fitted a single gaussian profile. Moreover, we have observed the NH_3 (2,2) transition towards the peak positions of the four molecular cores.

Table 2 displays the observed NH_3 (1,1) line parameters regarding the peak positions: the source name, the right ascension and declination offset ($''$) of the peak position with respect to the coordinates given in Table 1, the main beam brightness temperature, the LSR velocity (v_{LSR}; km s^{-1}), the apparent line width (FWHM; km s^{-1}) of the main component, the total optical depth and the intrinsic linewidth of the hyperfine components including instrumental broadening. The errors (r.m.s.) of the derived parameters are given in parentheses. Fig. 5 shows the NH_3 (1,1) and (2,2) spectra of the peak position of each mapped source. Table 3 lists the observed NH_3 (2,2) gaussian line parameters towards the NH_3 (1,1) peak positions: the main beam brightness temperature, the LSR velocity and the FWHM line width including instrumental broadening. For L1521D, we report the observed parameters towards the (+40, +20) peak position, since the integrated ammonia emission associated with this position is slightly larger that that of the (+80, +40) peak position.

Table 3. Observed NH_3 (2,2) line parameters

Name	$\Delta\alpha$ ($''$)	$\Delta\delta$ ($''$)	T_{MB} (K)	v_{LSR} (km s^{-1})	FWHM (km s^{-1})
L1521D	+40,	+20	0.5 (0.1)	6.81 (0.15)	0.6 (0.2)
L1521F	+20,	0	1.3 (0.2)	6.65 (0.15)	0.3 (0.2)
L1524	+20,	+20	0.9 (0.2)	6.44 (0.15)	0.3 (0.2)
L1507A	0,	+10	1.1 (0.3)	6.17 (0.15)	0.1 (0.2)

Table 4 gives the HC_5N (J=9–8) line parameters towards the ammonia peak positions, obtained from gaussian fits: the parameters are main beam brightness temperature, LSR velocity and FWHM line width including instrumental broadening. Fig. 6 shows the HC_5N (J=9–8) spectra.

5. Discussion

5.1. Derived parameters from NH_3 observations

The rotational temperature (T_{rot}) is defined by applying the Boltzmann distribution to the populations of different (J,K) rotational levels and has been calculated from the (1,1) and (2,2) data following the procedure outlined by Hüttemeister et al. (1993) and Lemme (1995). Given the rotational temperatures, it is possible to estimate the kinetic temperature (T_{kin}). Since the derived T_{rot} values (see Table 5) are all around 10 K, the differences between kinetic and rotational temperatures, as shown by Walmsley & Ungerechts (1983) and Danby et al. (1988), are

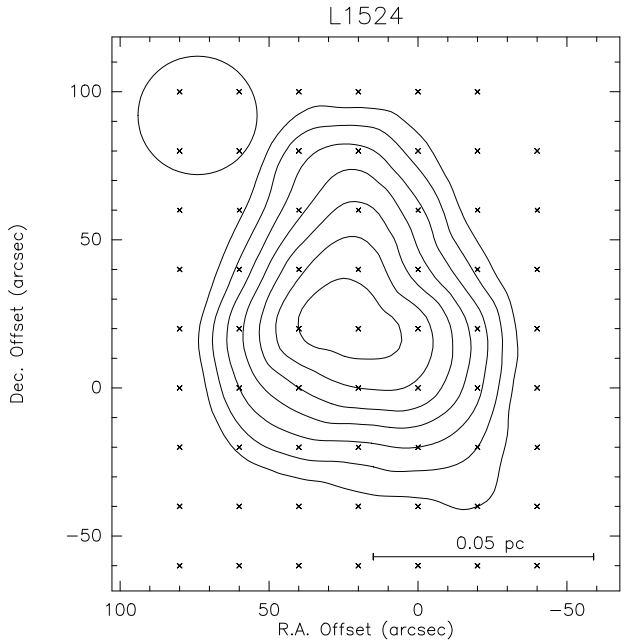

Fig. 3. Contour NH_3 (1,1) T_{MB} map of L1524. The (0,0) position corresponds to: $\alpha = 04^h\ 26^m\ 20^s$; $\delta = +24^\circ\ 28'\ 06''$. The contour levels are from 2.1 K to 4.5 K by steps of 0.4 K ($\simeq$ 2 r.m.s. noise). The empty circle shows the Effelsberg beam (HPBW).

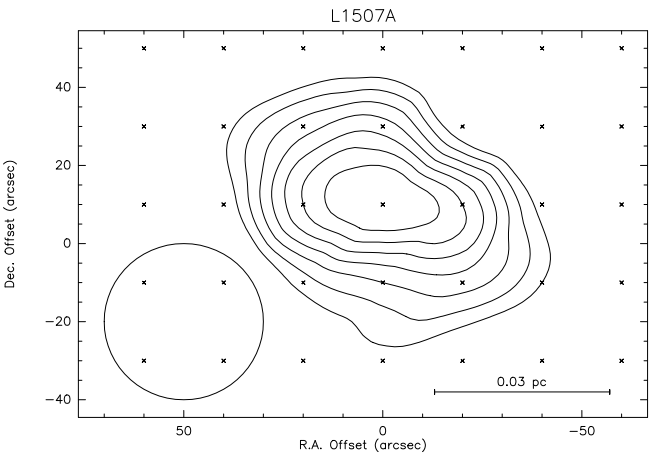

Fig. 4. Contour NH_3 (1,1) T_{MB} map of L1507A. The (0,0) position corresponds to: $\alpha = 04^h\ 39^m\ 29^s$; $\delta = +29^\circ\ 38'\ 07''$. The contour levels are from 2.0 K to 3.4 K by steps of 0.2 K ($\simeq$ 1 r.m.s. noise). The empty circle shows the Effelsberg beam (HPBW).

within the errors of our T_{rot} measurements. We thus can assume $T_{kin} = T_{rot}$.

The excitation temperature (T_{ex}), derived assuming a beam-filling factor of one, is defined in an analogous way to T_{rot}, but it is related to the population across an inversion doublet (J,K). Using T_{ex} and T_{rot}, it is possible to derive the total ammonia column density (N_{tot}; cm^{-2}) following the equations given by Ungerechts et al. (1986). For this, we have neglected non-metastable (J > K) inversion doublets and have assumed

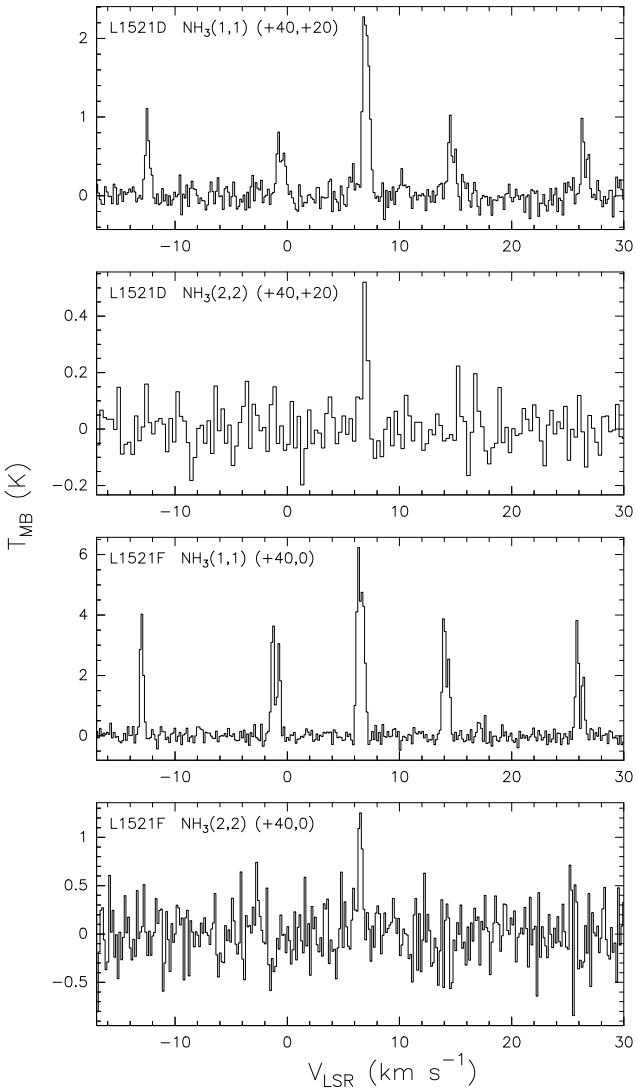

Fig. 5. Ammonia (1,1) and (2,2) spectra of the peak position of each mapped core. Source name and angular offset map position (in arcseconds) are indicated.

a common rotational temperature for all the metastable (J = K) states. These are reasonable approximations for rotational temperatures around 10 K (e.g. Harju et al. 1993). The derived temperatures and column density values (see Table 5) are consistent with NH_3 observations towards other molecular cores in the TMC (e.g. Myers & Benson 1983; Benson & Myers 1989) and more isolated Bok globules (Lemme et al. 1996; Scappini & Codella 1996). The measured (1,1) excitation temperatures are only slightly smaller than the rotational temperatures (see Table 5) suggesting that the (1,1) transition is close to being thermalised. $T_{ex} \simeq T_{rot}$ also requires that the beam-filling factor is near unity. This implies that, for the sources of the present sample, most of the ammonia flux is arising from an extended structure.

By balancing collisions and stimulated emission against spontaneous emission, the hydrogen density (n_{H_2}; cm^{-3}) can

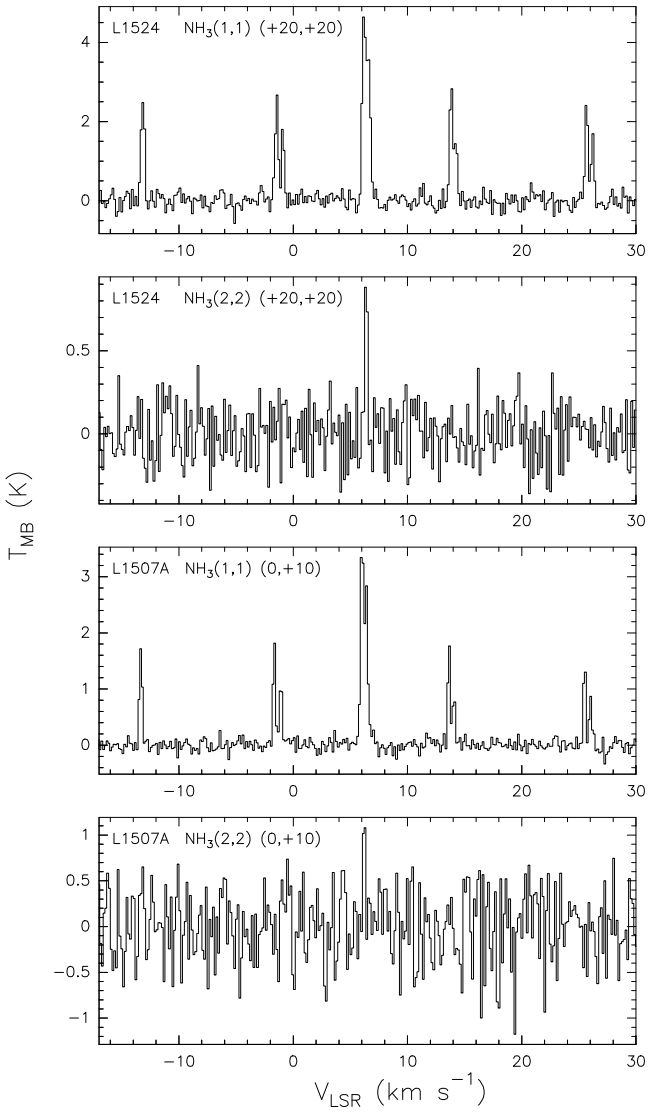

Fig. 5. (continued)

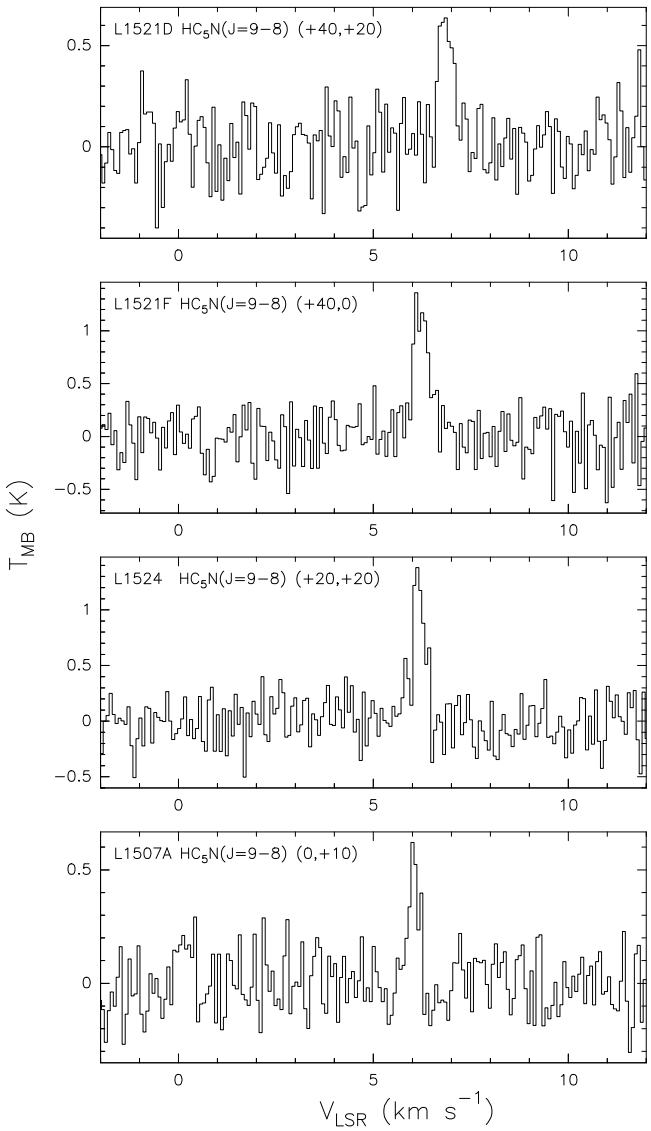

Fig. 6. Cyanodiacetylene (J=9–8) spectra at the ammonia peak position of each molecular core. Source name and angular offset (in arcseconds) relative to the (0,0) positions in the ammonia maps (see Figs. 1-4) are indicated.

be estimated (Ho & Townes 1983). The derived $n_{\rm H_2}$ values, also accounting for photon trapping, range from 0.6 10^4 to 19.9 10^4 cm^{-3} (see Table 6) and confirm that ammonia traces regions with densities $\geq 10^4$ cm^{-3}. Following Ho & Townes (1983), the errors on $n_{\rm H_2}$ are 17% and 64% for L1521D and L1507A, respectively. It is worth noting that the errors associated with $n_{\rm H_2}$ become large when $T_{\rm ex}$ is close to $T_{\rm rot}$. Thus, the hydrogen densities derived for L1521F and L1524, i.e. for those sources with $T_{\rm ex} \simeq T_{\rm rot}$, may be lower limits only.

It is well known that intrinsic motions in molecular clouds and, in particular, in molecular cores are complex. The spectral lines of thermally excited transitions also contain a non-thermal contribution to the linewidth (e.g. Myers et al. 1991), which can provide information about the dynamics of the molecular gas. In order to derive Δv, the *actual* intrinsic linewidth of the (1,1) line, we have corrected the observed intrinsic linewidth $\Delta v_{\rm INT}$ for the spectral resolution of the autocorrelator used during the observations, $\Delta v_{\rm aut}$, by means of $\Delta v^2 = \Delta v^2_{\rm INT} - \Delta v^2_{\rm aut}$, assuming the filter (and the line) being gaussian shaped. The actual intrinsic linewidth Δv is composed of a thermal component ($\Delta v_{\rm T}$) and a non-thermal one ($\Delta v_{\rm NT}$): $\Delta v^2 = \Delta v^2_{\rm T} + \Delta v^2_{\rm NT}$ (e.g. Myers et al. 1991). It is possible to see (Tables 2 and 5) that: (i) the actual intrinsic linewidths Δv are between 0.17 and 0.27 km s^{-1} ($\Delta v_{\rm INT} \simeq 0.28$ km s^{-1}) and (ii) the non-thermal velocity component is small, with a ratio between Δv and the thermal linewidth component $\Delta v/\Delta v_{\rm T} \simeq 1.3$. The results of the NH_3 observations, performed by Benson & Myers (1989) using the larger beamwidths of the Haystack and Green Bank antennas, indicate that, on average, ammonia cores with embedded IRAS source(s) have larger linewidths (0.45 km s^{-1}, not corrected for the spectral resolution) than cores without IRAS point

Table 4. Observed and derived HC_5N (J=9–8) line parameters

Name	$\Delta\alpha$ ($''$)	$\Delta\delta$ ($''$)	T_{MB} (K)	v_{LSR} (km s^{-1})	FWHM (km s^{-1})	N_{HC_5N} (10^{12} cm^{-2})
L1521D	+40,	+20	0.6 (0.2)	6.86 (0.09)	0.4 (0.1)	4.5 (0.7)
L1521F	+20,	0	1.2 (0.2)	6.22 (0.09)	0.5 (0.1)	9.2 (1.0)
L1524	+20,	+20	1.3 (0.2)	6.16 (0.09)	0.4 (0.1)	7.5 (0.9)
L1507A	0,	+10	0.6 (0.1)	6.03 (0.09)	0.3 (0.1)	1.6 (0.3)

source (0.27 km s^{-1}). Moreover, Myers et al. (1991) studied the linewidths of 61 dense condensations associated with star forming regions. They showed (see their Fig. 1) that the non-thermal component of the NH_3 core motions increases with IRAS luminosity more rapidly than does the thermal component and that in cores which can form stars more massive than 2 $M_\odot$, non-thermal motions dominate thermal motions ($\Delta v/\Delta v_T \simeq 4$). Thus, the linewidths derived suggest that our NH_3 clumps are either not associated with YSOs or that they are sites of low-mass star formation and are presumably associated with IRAS point sources of low luminosity ($L_{FIR} < 10\ L_\odot$; Myers et al. 1991), corresponding to a stellar mass of less than 2 $M_\odot$.

The LSR velocity information of the four mapped cores has been analysed in order to search for velocity gradients: v_{LSR} does not vary greatly within L1524 and L1507A, since the maximum differences between the v_{LSR} values of the map positions are 0.16 km s^{-1} and 0.14 km s^{-1}, respectively. These values are comparable to the channel spacing of 0.154 km s^{-1}. The map of L1521F shows a significant variation (0.46 km s^{-1}), but there is no clear indication for a systematic velocity gradient along a preferred axis. In contrast, L1521D displays a large variation of v_{LSR} across the map revealing a velocity gradient roughly along the north-south axis with a change of about 0.43 km s^{-1} over 120$''$ (cf. Fig. 1; weak line emission from outside the outer 1.4 K contour supports this trend). This corresponds to $\simeq 5$ km s^{-1} pc^{-1}, which is a value definitely larger than those reported by Goodman et al. (1993) for dense cores (< 4 km s^{-1} pc^{-1}). It is also worth noting that the direction of the gradient is not related to the major-axis of the elongated NH_3 distribution of L1521D (Fig. 1). This is consistent with the work of Goodman et al. (1993), who studied the occurrence of velocity gradients in a sample of 43 ammonia cores, suggesting that the motion connected with the gradient, either rotation or shear, is not the major factor in the core dynamics.

5.2. IRAS counterparts

It is well known that the IRAS PSC offers a precious opportunity to identify star forming regions in optically obscured objects, such as molecular cores. Using the IRAS PSC, Kenyon et al (1990) have recently performed a survey of star forming regions in the TMC, identifying about 100 YSOs. They have shown that YSOs are scattered in a large area of 15 pc $\times$ 20 pc and that star formation in the TMC is restricted to the dense molecular cores. With the aim to collect more information about the nature of the four molecular cores of the present list, we have cross-correlated their positions with the IRAS PSC. Clark (1987) has analysed the spatial distribution of 396 IRAS PS located up to 2 pc from 60 molecular cores. He found that the distribution is strongly peaked on the ammonia cores, with the central peak reduced by an order of magnitude at 0.18 pc. At distances larger than this value, a long tail is present and the population of IRAS PS can be significantly affected by background sources. Considering that the typical ammonia core diameter is 0.1 pc, 0.18 pc corresponds to 3.6 radii. Taking into account this result, we have looked for a coincidence within a radius of 1.8 times the size of the four molecular cores of the present sample. Moreover, IRAS sources known to be associated with extragalactic sources have been excluded (IRAS 1985). The result of the cross-correlation shows that L1521F and L1507A have no IRAS counterparts within the selected radius. We find two IRAS PS around L1521D, IRAS 04181+2655 (at a distance of 108$''$) and IRAS 04181+2654 (138$''$), and one near L1524, IRAS 04263+2426 (120$''$). It is worth noting that all these IRAS PS satisfy the typical IRAS colour distribution for IRAS counterparts of molecular cores, since they have [25-12] ([i-j] $\equiv \log [F_i/F_j]$, where $F_{i,j}$ are the IRAS flux densities in bands i and j, in μm) in the range between 0.42 and 0.47 and [60-12] between 0.60 and 1.23 (for comparison, see figure 3 of Codella & Palla 1995).

We thus conclude that L1521D and L1524 are associated with at least one IRAS counterpart (and therefore presumably with YSOs), while L1521F and L1507A appear not to be connected with any IRAS PS. Following Henning et al. (1990), the IRAS luminosities of the associated IRAS PS has been computed. The values of L_{FIR} are 0.3 $L_\odot$ for IRAS 04181+2655 and IRAS 04181+2654 (L1521D) and 6.1 $L_\odot$ for IRAS 04263+2426 (L1524). This confirms that the ammonia molecular cores are sites of low-mass star formation, in accord with our results from the ammonia linewidths (Sect. 5.1).

5.3. NH_3 core stability

In order to obtain estimates of the energy terms of the NH_3 cores of our sample, the *mean* NH_3 total column density has been obtained as the average of all observed positions inside the FWHP contour of the ammonia cores (Figs. 1–4). This allows to calculate, using the ammonia abundance and assuming spherical cloud geometry, estimates of the *mean* hydrogen density and of the mass M ($M_\odot$) of a molecular core (Table 6). It is worth noting that, since M has been derived from the NH_3 total column density without virial equilibrium, we have made no assumption about the stability of the NH_3 cores. Ammonia abundances in interstellar molecular clouds cover a wide range:

Table 5. Derived parameters from NH_3 observations

Name	T_{rot} (K)	T_{ex} (K)	N_{11} (10^{14} cm^{-2})	N_{tot} (10^{14} cm^{-2})	Δv (km s^{-1})	Δv_T (km s^{-1})	Δv_{NT} (km s^{-1})
L1521D	9.9 (1.2)	6.0 (0.2)	1.2 (0.3)	5.4 (1.8)	0.27 (0.02)	0.16 (0.02)	0.22 (0.02)
L1521F	9.1 (1.0)	9.0 (0.3)	3.8 (0.3)	20.1 (1.6)	0.17 (0.01)	0.16 (0.01)	0.06 (0.01)
L1524	7.9 (0.7)	7.5 (0.2)	3.8 (0.3)	27.7 (6.6)	0.18 (0.01)	0.15 (0.01)	0.10 (0.01)
L1507A	8.9 (1.7)	6.8 (0.3)	1.5 (0.2)	8.3 (3.6)	0.20 (0.01)	0.15 (0.02)	0.13 (0.02)

the $[NH_3]/[H_2]$ ratio is believed to vary from a few 10^{-8} in small dark clouds up to 10^{-5} in the dense cores like Orion-KL (e.g. Ho & Townes 1983 and references therein). In particular, Benson & Myers (1983) studied the NH_3 abundance in a sample of quiescent dense molecular clouds and found that $[NH_3]/[H_2]$ ranges between 3 10^{-8} and 2 10^{-7}.

In order to derive the parameters reported in this paper, we have assumed $[NH_3]/[H_2] = 10^{-7}$. The resulting masses lie between 0.2 and 1.0 $M_\odot$, placing the NH_3 cores with the lowest M values (L1507A and L1521D) towards the edge of the mass distribution for ammonia cores in the TMC, which ranges from a fraction to a few tens of solar masses, with a median value of 4 $M_\odot$ (Benson & Myers 1989).

Studying C_3H_2 and $H^{13}CO^+$ in TMC molecular cores, Mizuno et al. (1994) found that, contrary to the NH_3 results of Benson & Myers (1989), the cores without young stars (i.e. IRAS counterparts) are less dense than those with stars. The results of Mizuno et al. (1994) and Benson & Myers (1989) are consistent (average values) regarding the hydrogen density of the cores not connected with stars (4 10^4 and 3 10^4 cm^{-3}, respectively), while for those which host YSOs Mizuno et al. (1994) find $n_{H_2} \simeq 5\ 10^5$ cm^{-3}, a value larger than that given by Benson & Myers (1989), 1 10^4 cm^{-3}. It is worth noting that Mizuno et al. (1994) determined the hydrogen density from $H^{13}CO^+$ data, while the Benson & Myers (1989) analysis is based on a large velocity gradient model for the NH_3 cores. Mizuno et al. (1994) suggest that the disagreement of their results with those of Benson & Myers (1989) could be caused by differences in angular resolutions: 20″ vs. 1′.2, respectively. We stress that our results have been obtained with a resolution of 40″, which is still lower that that of the Mizuno et al. (1994) observations, but which is definitely higher than that used by Benson & Myers (1989). The hydrogen densities derived from our data show no remarkable difference between the n_{H_2} values of NH_3 cores with (L1521D and L1524) or without (L1521F and L1507A) IRAS counterparts.

In Table 6 we display the energy terms of the cores of our sample: turbulent (E_{tu}; J), thermal (E_{th}; J) and gravitational (E_{gr}; J). The last column is for the parameter $\alpha \equiv E_{gr}/(E_{tu} + E_{th})$, which is a measure of core stability. The turbulent, thermal and gravitational (assuming a homogeneous sphere) energy terms have been derived using the formulae reported by Harju et al. (1993).

Star formation occurs most readily in molecular clumps in which the internal motions are sufficiently reduced to allow the occurrence of gravitational collapse. Table 6 shows that the thermal energy is always larger than the turbulent one. The values of α for the four cores lie between 0.2 (L1521D) and 1.2 (L1524); $\alpha = 1$ implies gravitational equilibrium in the absence of a magnetic field. The values obtained here are only slightly different from unity. Taking into account the contribution of a magnetic field to the energetic support against gravitational collapse, considering also uncertainties in the assumed $[NH_3]/[H_2]$ value and deviations from the adopted (spherical) geometry of the cores, we can conclude that the four ammonia cores are close to equilibrium. These considerations are in agreement with the results of Myers & Goodman (1988) and Harju et al. (1993) who found that the NH_3 cores in the TMC are approximately virialized.

Table 6. Derived parameters related to the core stability of the NH_3 condensations

Name	n_{H_2} (10^4 cm^{-3})	M ($M_\odot$)	E_{tu} (10^{34} J)	E_{th} (10^{34} J)	E_{gr} (10^{34} J)	α
L1521D	0.6	0.3	0.9	3.5	0.9	0.2
L1521F	19.9	0.7	0.8	7.9	7.4	0.9
L1524	2.5	1.0	1.0	8.9	11.8	1.2
L1507A	1.1	0.2	0.2	2.2	1.2	0.5

5.4. Derived parameters from HC_5N observations

An estimate of the total HC_5N column density (N_{HC_5N}; cm^{-2}) has been derived through the standard equation (e.g. Olano et al. 1988), using the molecular parameters given, e.g., by Alexander et al. (1976) and Churchwell et al. (1978). Table 4 lists the derived cyanodiacetylene column densities at the ammonia peak positions of the four molecular cores: the values range from 1.6 10^{12} to 9.2 10^{12} cm^{-2}, in agreement with the N_{HC_5N} values of other molecular cores located in the TMC (Benson & Myers 1983).

In order to estimate the HC_5N abundances a comparison between HC_5N and NH_3 column densities has been made. We presently do not know the size and geometry of the HC_5N distribution in the ammonia cores. However, the HC_5N and NH_3 maps given by Benson & Myers (1983) show that the size and shape of the maps are similar and that the peak positions differ significantly only for the TMC-1 molecular core. Therefore, we have estimated the $[HC_5N]/[H_2]$ ratio using the cyanodiacetylene and ammonia column densities and the NH_3 abundance. The obtained $[HC_5N]/[NH_3]$ values are: 8.3 10^{-3} (L1521D), 4.6 10^{-3} (L1521F), 2.7 10^{-3} (L1524) and 10.7 10^{-3} (L1507A). Thus, the derived HC_5N abundances relative to H_2 are: 8.3 10^{-10}

(L1521D), 4.6 10^{-10} (L1521F), 2.7 10^{-10} (L1524) and 1.1 10^{-9} (L1507A), in agreement with the suggestion of Benson & Myers (1983), that relative cyanodiacetylene abundances in dense cool cores vary from $\simeq 10^{-10}$ to $\simeq 10^{-9}$.

6. Conclusions

We have investigated 4 dense ammonia cores (L1521D, L1521F, L1524 and L1507A) in the TMC, increasing the number of known such objects to 20 in this prototypical dark cloud complex. The main results of our study can be summarized as follows:

1. The ammonia observations reveal clumps with sizes of 0.06-0.09 pc and yield kinetic temperatures between 7.9 and 9.9 K. The actual intrinsic linewidths are between 0.17 and 0.27 km s^{-1}, while the thermal linewidths are around 0.15 km s^{-1}. Therefore, the non-thermal velocity component is rather small. The ratio between the intrinsic and thermal linewidth is about 1.3, indicating that only low-mass stars can eventually form in these NH_3 cores. This is also supported by the association of two of the NH_3 cores with low luminosity IRAS counterparts ($L_{\rm FIR} < 10\ L_{\odot}$).
2. The NH_3 data show that the measured (1,1) excitation temperatures are only slightly smaller than the rotational temperatures suggesting that the (1,1) inversion transition is close to being thermalised. From the peak NH_3 emission hydrogen densities (between 0.6 and 19.9 10^4 cm^{-3}) have been estimated. Moreover, from the average of all observed positions inside the FWHP contour of the ammonia cores, the core masses (0.2 – 1.0 $M_{\odot}$) have been estimated. The derived hydrogen densities show no remarkable difference between NH_3 cores with or without IRAS counterparts. The low M values place the four objects towards the edge of the M distribution for ammonia cores in the TMC, which ranges from fractions to few tens of solar masses, with a median value of 4 $M_{\odot}$.
3. Estimates of the turbulent, thermal and gravitational energy have been derived. The thermal energy is always larger than the turbulent one. The four cores may be close to equilibrium.
4. Emission at 24.0 GHz, caused by the J=9–8 transition of HC_5N, has been detected towards the ammonia peak positions of the four molecular cores. This increases the number of known such objects from 11 to 15 in the TMC (cf. Benson & Myers 1980, 1983). The derived HC_5N column densities range between 1.6 10^{12} and 9.2 10^{12} cm^{-2}, in agreement with results of previous HC_5N observations in the TMC.

Acknowledgements. The authors like to thank M. Walmsley for valuable discussions and suggestions.

References

Alexander A.J., Kroto H.W., Walton D.R.M., 1976, J. Molec. Spectrosc. 62, 175
Baars J.W.M., Genzel R., Pauliny–Toth I. I. K., Witzel A., 1977, A&A 61, 99
Beichman C.A., Jennings R.E., Emerson J.P., et al., 1984, ApJ 278, L45
Beichman C.A., Myers P.C, Emerson J.P., et al., 1986, ApJ 307, 337
Benson P.J., Myers P.C., 1980, ApJ 242, L87
Benson P.J., Myers P.C., 1983, ApJ 266, 309
Benson P.J., Myers P.C., 1984, ApJ 270, 589
Benson P.J., Myers P.C., 1989, ApJS 71, 89
Blaauw A., 1991, in "The Physics of Star Formation and Early Stellar Evolution", Eds C.J. Lada & N.D. Kylafis (Dordrecht: Kluwer), 125
Churchwell E., Winnewisser G., Walmsley C.M., 1978, A&A 67, 139
Clark F.O., 1987, A&A 180, L1
Codella C., Palla F., 1995, A&A 302, 528
Danby G., Flower D.R., Valiron P., Schilke P., Walmsley C.M., 1988, MNRAS 235, 229
Fukui Y., 1989, in "Low Mass Star Formation and Pre-Main-Sequence Objects", Ed. B. Reipurth (Garching bei München: ESO), 95
Fukui Y., Iwata T., Mizuno A., Bally J., Lane A.P., 1993, in "Protostars and Planets III", Eds. E.H. Levy & J. Lunine (Tucson: Univ. Arizona Press), 603
Fuller G.A., 1989, PhD thesis, Astron. Dept. Univ. of California, Berkeley
Fuller G.A., Myers P.C., 1993, ApJ 418, 273
Goodman A.A., Benson P.J., Fuller G.A., Myers P.C., 1993, ApJ 406, 528
Harju J., Walmsley C.M., Wouterloot J.G.A., 1993, A&AS 98, 51
Henning T.H., Pfau W., Altenhoff W.J., 1990, A&A 227, 542
Hüttemeister S., Wilson T.L., Henkel C., Mauersberger R., 1993, A&A 276, 445
Ho P.T.P., Townes C.H., 1983, ARA&A 21, 239
IRAS Point Source Catalogue, 1985, Joint IRAS Science Working Group (U.S. GPO, Washington)
Lemme C., 1995, Ph.D. thesis, Univ. Bonn, Germany
Lemme C., Wilson T.L., Trieftrunk A.R., Henkel C., 1996, A&A 312, 585
Kenyon S.J., Hartmann L.W., Strom K.M., Strom S.E., 1990, AJ 99, 869
Mizuno A., Onishi T., Yonekura Y., et al., 1994, Nat 368, 719
Mizuno A., Onishi T., Hayashi M., et al., 1995, ApJ 445, L161
Myers P.C., Benson P.J., 1983, ApJ 266, 309
Myers P.C., Goodman A.A., 1988, ApJ 329, 392
Myers P.C., Ho P.T.P., Benson P.J., 1979, ApJ 233, L141
Myers P.C., Linke R.A., Benson P.J., 1983, ApJ 264, 517
Myers P.C., Ladd E.F., Fuller G.A., 1991, ApJ 372, L95
Olano C.A., Walmsley C.M., Wilson T.L., 1988, A&A 196, 194
Onishi, T., Mizuno, A., Kawamura, A., Ogawa, H., Fukui, Y., 1996, ApJ 465, 815
Scappini F, Codella C., 1996, MNRAS 282, 587
Strom K.M., Strom S.E., Edwards S., Cabrit S., Skrutskie M.F., 1989, AJ 97, 1451
Ungerechts H., Thaddeus P., 1987, ApJS 63, 645
Ungerechts H., Walmsley C.M., Winnewisser G., 1982, A&A 111, 339
Ungerechts H., Walmsley C.M., Winnewisser G., 1986, A&A 157, 207
Walmsley C.M., Ungerechts H., 1983, A&A 122, 164
Walmsley C.M., Winnewisser G., Toelle F., 1980, A&A 81, 245
Weintraub D.A., 1990, A&AS 74, 575
Wouterloot J.G.A., Habing H.J., 1985, A&AS 60, 43
Wouterloot J.G.A., Brand J., Fiegle K., 1993, A&AS 98, 589

This article was processed by the author using Springer-Verlag LaTeX A&A style file *L-AA* version 3.